V_P/V_S from prestack multicomponent seismic data and automatic PS to PP time mapping

Osareni C. Ogiesoba[1] and Robert R. Stewart

ABSTRACT

This paper discusses the development and application of a prestack method that scans for the average vertical velocity ratio (V_P/V_S) value, generally referred to as γ_0, and the stacking velocities of multicomponent seismic data using a converted-wave (*PS*) non-hyperbolic traveltime equation. The procedure entails computing semblance as a function of two variables namely, the PS stacking velocity V_{PS}, and γ_0, with respect to the *PS* zero-offset time t_{ps0}. The results are displayed in 2D plots. We tested the procedure using numerical data sets and real data sets from the Blackfoot Field in Southern Alberta. We observed that the γ_0 values from the scanning method agree reasonably well with theγ_0 values from the well log of Well 09-08 located at the CDP location at which the analysis was performed. In addition, when these γ_0 estimates are used for *PS*-*PP* time mapping, the time difference between the computed and actual *PP* time at the target level is found to be 10 ms; being an error of less than 3%.

INTRODUCTION

A number of authors (e.g. Stewart et al, 2003) have discussed the benefits offered by *PS*-wave exploration; however, the realization of these benefits is dependent on overcoming certain problems that mitigate against *PS*-wave data. One of such problems and probably the most important, is determining the correct value/s of γ_0 at which *P*-wave converts to *S*-wave. Because of this, recovery of γ_0 has become a step in multi-component data processing and interpretations. Several authors have used different methods for the recovery of γ_0, for example, Gaiser (1996) developed a post-stacked cross-correlation method. The method is automatic and is based on correlating *PP* and *PS* stacked data sets. Thomsen (1999) suggested visually correlating events of the same structural attitude on both *PP* and *PS* stacked section. Li et al., (1999; 2001) discussed a prestack method via velocity analysis but concluded that it was not possible to recover γ_0 using this procedure. Stewart et al. (2003) alluded to a time-isochron method using interpreted *PP* and *PS* sections. Like Gaiser's method, this too is a post-stack method that depends on correlating *PP* and *PS* events. The post-stack methods can work well but may fail with complicated sections, when *PP* and *PS* data have very different wavelets, or events of opposite polarity. And as noted by (McCormark et al., 1984; Garotta, 1985; Tessmer and Behle, 1988), these post-stack methods can introduce errors due to miscorrelation. For example, problems caused by different tuning effects with respect to thin beds for different wave types can lead to miscorrelation of *PP* and *PS* stacked data sets. Furthermore, effects of anisotropy and insufficient S-wave static corrections can as well lead to miscorrelation (Tessmer and Behle, 1988). Also, in areas of flat-lying geology, like in Western Canada, events can look the same. Furthermore, different statics and datums may significantly shift the sections from each other; therefore, recognizing similar structures on the *PP* and *PS* sections becomes a problem. In view of these, there is

[1] Seismic Research Group, Earth and Planetary Sciences, McGill University

need to find an alternate prestack solution to the problems associated with *P*- and *PS*-wave correlation.

In this paper, we present a prestack method of estimating $\gamma_0$via velocity analysis using Thomsen (1999) converted-wave non-hyperbolic traveltime equation. By using the *PS* stacking velocity approximation of Tessmer and Behle (1988) in the traveltime equation, the variables to be scanned for are reduced from 3 to 2. Stewart and Ferguson (1996) used similar approximations to derive shear-wave interval velocities from *PS*-wave data sets in Southern Alberta. Though Thomsen's equation is designed for a single isotropic layer, it works reasonably well in multilayer case as we discuss hereunder.

CONVERTED-WAVE TRAVELTIME EQUATION

For a single isotropic layer, PS-wave traveltime equation as derived by Thomsen (1999) can be written as:

$$t_{PS}{}^2(x) = t_{PS0}{}^2 + \frac{x^2}{V_{PS}{}^2} - \left(\frac{(\gamma_0 - 1)^2 (V_P{}^2 - V_{PSs}{}^2)}{4(V_P{}^2 - V_{PS}{}^2)(\gamma_0 + 1) t_{PS0}{}^2 V_{PS}{}^4 + (\gamma_0 - 1)^2 V_P{}^2 V_{PS}{}^2 x^2} \right) x^4, \quad (1)$$

where x is the offset, t_{PS0} is the *PS*-wave zero-offset traveltime, V_P and V_{PS} are respectively the *P*-wave and *PS*-wave moveout velocities and γ_0 is the velocity ratio. It is impracticable to use Equation 1 for velocity analysis since it contains three unknown variables: V_P, V_{PS}, and γ_0. Thus, to simplify the expression, we utilized the Tessmer and Behle (1988) approximation:

$$V_{PS}{}^2 \cong \frac{V_P{}^2}{\gamma_0}. \quad (2)$$

Equation 2 is based on the assumption of horizontally layered and isotropic earth. By substituting Equation 2 into Equation 1, the traveltime equation becomes:

$$t_{PS}{}^2(x) = t_{PS0}{}^2 + \frac{x^2}{V_{PS}{}^2} - \left(\frac{(\gamma_0 - 1)^2}{4(\gamma_0 + 1) t_{PS0}{}^2 V_{PS}{}^4 + \gamma_0 (\gamma_0 - 1) V_{PS}{}^2 x^2} \right) x^4. \quad (3)$$

As can be seen from Equation 3, the *PS*-wave traveltime equation now contains two unknown parameters and the velocity is expressed in *PS*-wave stacking velocity compared to Equation 2 which has three variables. One may ask if Equation 3 can adequately describe converted-wave traveltimes.

Validity of PS traveltime equation

We tested the validity of Equation 3 by first creating a numerical model (Figure 1), from which we obtained PS synthetic seismic records (Figure 2a). Both Figures 1 and 2a were generated using ANIVEC, a frequency-wave number based modeling package. The numerical model consists of a single isotropic medium; the acquisition geometry consists of 60 geophones spaced at 100 m with a maximum offset of 6 km. Next, we used the model parameters in Equation 3 to compute traveltimes which are then plotted against

offsets; the result of this procedure is shown in Figure 2b. The numerical traveltime values from ANIVEC and those obtained from the synthetics generated by using Equation 3 are compared in Tables 1 and 2. The average percentage error between the traveltimes obtained by using Equation 3 and those from ANIVEC for the first 10 offsets is 0.04%; while the error from the last 10 offsets is 0.4%. This comparison shows that the values from Equation 3 and those from ANIVEC are quite close.

Senssitivity test

Having tested the validity of the traveltime equation for this straightforward case, we carried out a sensitivity analysis to see the effect of the variations in γ_0 and V_{PS} on moveout. This test was performed by generating traveltime curves, first at constant γ_0 while varying the *PS*-wave velocity; and secondly, by fixing the PS-wave velocity and varying γ_0. The results of these tests are shown in Figure 3. From this Figure, we observed that moveout changes significantly with variations in velocity. On the other hand, the changes in moveout due to γ_0 variations are less dramatic compared to those observed in velocity variations. This implies that moveout is more sensitive to velocity than γ_0 In spite of this moveout still has enough sensitivity due to γ_0 variations to be exploited for the purposes of γ_0 scanning via velocity analysis.

Dual parameter algorithm development

We utilized the Tanner and Koehler (1969) semblance equation and Equation 3 above in the development of the Scanning code and computed semblance as a function of *PS* velocity, velocity ratio (γ_0), and the zero-offset two-way time (t_{PS0}). To extract γ_0, we sub-divided the entire semblance volume into n sub-volumes (Figure 4), and computed 3D semblance within each sub-volume. 2D semblance display for each volume is obtained by summing semblances along the γ_0 axis and dividing by the number of γ_0 to obtain average semblance in two-dimensional sense. The 2D semblance panel corresponds to the average γ_0 within each sub-volume (Figure 5). That is, if there are say *n* sub-volumes, there will be *n* γ_0 values corresponding to *n* semblance panels. For each time-velocity coordinate pair, a search for maximum semblance is performed amongst all the *n* panels. The γ_0 value, at which the maximum semblance is found, is output onto a γ_0 panel; while the maximum semblance value is output onto a semblance panel. The end result will be a final 2D velocity semblance panel and a 2D γ_0 panel (Figure 6). From the final 2D velocity semblance panel, pick velocity-time pairs that correspond to maximum semblance. Interpolate picked values according to the seismic sampling rate to obtain a continuous time-velocity function. The function is automatically transferred to the γ_0 panel from whence corresponding γ_0 values are picked automatically and plotted to give a continuous γ_0-time log (Figure 6). Based on the above concepts we developed Matlab codes and applied them to numerical and real data sets to scan for the stacking velocities and γ_0 values.

APPLICATION OF THE SCANNING ALGORITHM: NUMERICAL MODEL

Our numerical data sets consist of synthetic shot records obtained from a 3-layer isotropic geologic model (Figure 7) constructed using the GX2 raytracing modeling package. The synthetic shots gathers were generated using a Ricker wavelet of 30 HZ dominant frequency. We adopted a split-spread shooting pattern and acquired 41 shot records for *P*- and *PS*-wave the maximum spread length and receiver spacing being 4000 m and 100 m respectively. Examples of the *P*- and *PS*-wave shot records are shown in Figure 8. The computed two-way zero-offset traveltimes and the average vertical velocity ratios are shown in Table 3. We compute the *P*- and *S*-wave RMS velocities using Dix's equation,

$$V_{rms}^{\ 2} = \frac{\sum_{i=1}^{N} t_i v_i^{\ 2}}{\sum_{i=1}^{N} t_i}, \tag{4}$$

where i is the interval and N is the number of intervals. Results from Equation 4 are fed into Equation 5 to compute the *PS* RMS velocities;

$$V_{PS} = \left[\frac{t_P V_P^{\ 2} + t_S V_S^{\ 2}}{t_{PS}} \right]^{0.5}, \tag{5}$$

where V_{PS}, V_P and V_S are respectively the *PS*-, *P*- and the *S*-wave RMS velocity, and t_{PS}, t_P and t_S are the *PS*-, *P*- and *S*-wave total one-way time respectively. Computed RMS velocities are shown in Table 4.

Next, we exported the shot gathers to ProMAX seismic processing environment for processing from whence a PS-wave shot gather is sent to Matlab for semblance computation and velocity ratio extraction. Following the procedures discussed above, we subdivided the entire semblance volume into 10 sub-volumes and computed 3D semblance within each volume. Values of γ_0 employed in the scanning range from 2.0 to 2.26 sampling at 0.005 intervals; while velocities vary from 1900 to 2600 m/s and at intervals of 100 m/s. Displayed in Figure 9 are the 2D semblance plots from 3 sub-volumes. In this Figure, it can be seen how moveout varies due to the variations in velocity ratio. From the final 2D velocity semblance panel, we picked maximum semblance at the different horizons and transfer the corresponding time-velocity coordinate pairs to the 2D velocity ratio panel. Velocity ratio values encountered at the coordinate locations are automatically plotted (Figure 10). In this figure, the final 2D semblance panel is displayed together with the 2D velocity ratio panel and γ_0-time log. In this simple multi-layer case, the γ_0-time log is a series of spikes at the various level; the scanned γ_0 values starting at the shallowest to the deepest level are: 2.160, 2.230 and 2.210. The results are tabulated in Tables 5 to 7.

Having scanned for the velocity ratios, we processed the data sets in ProMAX to obtain the *P*- and *PS*-wave stacked sections (Figure 11). By applying the Tessmer and Behle (1988) *PS*- to *P*-wave time transforming-equation

$$t_{P0} = (2 * t_{PS0}) / (1 + \gamma_0), \quad (6)$$

and the scanned velocity ratio values, we transformed the *PS*-wave stacked section to *P*-wave times (Figure 11). The velocity ratio function used in the transformation is shown in Figure 11. The differences between the computed *P*-wave times and the actual are shown in Table 8, and vary from 0.2 to -3.0%. This shows that the computed results closely agree with the actual values.

APPLICATION OF THE SCANNING ALGORITHM: REAL DATA SET EXAMPLE

Our real data set is a 3C seismic line from the Blackfoot Field in South Central Alberta. The Blackfoot Field reservoir is located in one of the incised channels within the Mannville Group of Lower Cretaceous age. It is overlain by the Colorado Group of Lower to Upper Cretaceous age. Both the Mannville and the Colorado Groups are composed of essentially siliciclastic sediments. The Mannville Group is uncomformably underlain by the Mississippian which is mostly of carbonate lithology. Structurally, the area is essentially of flat-lying geology.

The 3C seismic data was acquired by the CREWES Project in 1997; the maximum spread is about 3000 m with the receiver and shot spacing being 20 m each. Along the line of traverse, is the hydrocarbon-bearing Well 09-08. The well has a gamma-ray log and V_P/V_S log derived from VSP.

For the velocity ratio exercise, we processed the data set in ProMAX and extracted ACP gathers using an initial velocity ratio value of 2.1 to bin data. We then exported traces from ACP 350, which is at the Well 09-08 location, into Matlab for velocity analysis and velocity ratio scanning. In this data set example, we used a range of γ_0 values from 1.5 to 3.0, and sampling at 0.025 intervals. The velocities ranged from 500 m/s to 4500 m/s, at intervals of 25 m/s. The time ranged from 0.02 second to the end of the record time (4.0 seconds) sampling at intervals of 0.02 second. We subdivided the whole volume into 11 sub-volumes to give 11 2D velocity semblance panels. From these, we obtain the final 2D velocity semblance and the 2D γ_0 panels as discussed already. Using the final 2D semblance display, we picked the stacking velocities and the corresponding two-way times. These time-velocity coordinate pairs are then transferred to the 2D γ_0 panel from whence associated γ_0 values are automatically picked and plotted. Results are shown in Figures 12 and 13.

Figure 12 shows the 2D velocity semblance from sub-volumes 1 and 11. The variation of maximum semblance at the various horizons can clearly be seen especially at shallow levels; with the low V_P/V_S value of 1.5, there appears to be scattering of events at shallow levels; whereas with a V_P/V_S value of 2.8, there appears to be better alignment of events. In Figure 13b the final 2D velocity semblance panel, events are better aligned than they are in either Figure 12a, or 12b.

DEPTH CONVERSION AND COMPARISON OF SCANNED VP/VS WITH WELL 09-08 RESULTS

To test the accuracy of the scanned V_P/V_S log, we compared the results with the V_P/V_S log from the Well 09-08. In order to carry out this comparison, we derived an equation to convert the *PS*-wave velocities and times into depth since the Well 09-08 log is in depth. We derive the depth conversion equation as follows:

Since the area of work is essentially of flat-lying geology, we assume that the P-wave stacking velocity is approximately equal to the average velocity (Al Chalabi, 1974). From Equation 2,

$$V_P \cong V_{PS}\gamma_0^{\,0.5}. \tag{7}$$

Combining Equations 6 and 7, and dividing the two-way traveltime by 2 we have,

$$Depth = \frac{1}{2}(V_P t_{P0}) = \frac{V_{PS} t_{PS0} \gamma_0^{\,0.5}}{1+\gamma_0}. \tag{8}$$

Using Equation 8 and the *PS*-wave stacking velocities, the corresponding times are transformed to depths; computed depth values are then plotted against corresponding γ_0 values. The resultant γ_0-log plot corresponding to the same depth range of Well 09-08 is compared with the γ_0-log plot from the well in Figure 14. Also shown in Figure 14 is the plot of Well 09-08 gamma-ray log (pink curve) and the V_P/V_S log (blue curve). The depth (about 816 m), at which these two logs cross each other, indicate major lithologic boundary. In this Figure, the correspondence between the scanned V_P/V_S log (purple curve) and the V_P/V_S log from Well 09-08 is quite reasonable. The depth point at which the gamma-ray log switches from shale-dominated to sand-dominated interval can clearly be seen on both the scanned and the Well 09-08 V_P/V_S log. The sand-dominated interval corresponds to low V_P/V_S values, while the shale-dominated interval corresponds to high V_P/V_S values. The implication of this is that, given a *PS*-wave data, it is possible to predict lithology via prestack velocity ratio scanning discussed above.

PS TO PP TIME MAPPING

PS to *PP* time mapping was carried out in three stages; first we processed the data sets in ProMAX from whence we obtained the *PP* and *PS* migrated stacked sections (Figures 15 and 16). Next we smoothed the V_P/V_S-time log shown in Figure 13d using a 15-point moving average operator and use the result in Equation 6 to get the *P*-wave times. Finally we applied these times to the *PS*-migrated stacked section by plotting the *PS*-wave amplitudes versus the computed *P*-wave times. The results of these procedures are shown in Figure 17. A comparison of the *PP* and the transformed *PS* stacked sections at the Well 09-08 location (CDP 350) is shown in Figure 18; the figure indicates that there is an error of about 10 to 15 ms miss-tie between the *PP* (Figure 18a) and the *PS* (Figure 18b) stacked sections. Overall, there is a reasonably good tie of *PP* and *PS* events even at times of 1.5 to end of record time. Previous multi-component seismic interpretation of the study area by the CREWES Project in 1996 identified the top of a channel (the Viking Channel) to be at about 1.00 seconds *P*-wave time (1.510 seconds *PS* time); this time

pick is indicated in Figure 18 by the yellow lines. From Figure 18, the percentage error between the pick of the channel top in the *PP* and in the *PS* sections is less than 3%.

DISCUSSION

The traveltime equation utilized in designing the scanning algorithm was derived for a single, isotropic layer. However, it works reasonably well in multilayer case as has been shown in this paper. From the validity tests above, errors in traveltimes become significant at far-offsets (offsets greater than 3 km as in this case). At about 4 kilometers, the average observed traveltime error was 0.4% (error associated with the last 10 offsets). This implies that we need an improved traveltime equation to handle the long offset events. However, by increasing the number of sub-volumes in the scanning process, the errors in velocity ratios are minimized. In applying the scanned velocity ratios in *PS* to *PP* transformation, it is necessary to smooth the curve to ensure a smooth transformation; the smoother the curve, the better is the transformation. The 10 to 15 ms miss-tie that is observed between the *PP* and the transformed *PS* stacked sections in Figure 18, is probably due to inadequate smoothening as well as errors due to the traveltime equation. Nevertheless, the scanning procedure still works well and can be applied in areas of relatively flat-lying geology. The advantage in this process is that velocity ratios can be scanned for during velocity analysis at minima cost; that is, as the stacking velocities are picked, the velocity ratios are automatically obtained the same time.

CONCLUSIONS

This study has demonstrated a number of aspects. The sensitivity analysis shows that moveout is more sensitive to changes in velocity than it is to changes in velocity ratios; however, by carefully designing a searching algorithm, the sensitivity of moveout due to the changes in velocity ratios can still be detected. The traveltime equation utilized in this study is adequate to describe converted wave events. There is about 0.4% error associated with the far-offsets events. Thus, an improved traveltime equation that would handle far-offsets events would also improve values of scanned velocity ratios.

The results from both the synthetic and real data sets used in this study have shown that it is possible to perform a prestack velocity ratio scanning using velocity analysis. In both cases, the error incurred when the scanned velocity ratio values are used in *PS*-to-*P* time transformation is less than 4%. In the real data set example, the scanned velocity ratio log is reasonably in good agreement with the velocity ratio log from the well (Well 09-08). However, there is more work to be done in converted-wave prestack velocity ratio estimation.

ACKNOWLEDGEMENTS

We would like to express our deep gratitude to the sponsors of the Consortium for Research in Elastic Wave Exploration Seismology (CREWES Project) for supporting this project. Many thanks to WesternGeco staff, James Gaiser and Rich Van Dok, for allowing us to use the ANIVEC software in our study. We are also grateful to the staff and students of CREWES. We thank Richard Bale and Carlos Nieto for their useful suggestions.

REFERENCES

Al Chalabi, M., 1974, An analysis of stacking, RMS, average and interval velocities over a horizontally layered ground: Geophys. Prosp., **22**, 458-475.

Gaiser, J.E., 1996, Multicomponent Vp/Vs correction analysis: Geophysics, **61**, 1137-1149.

Garotta, R., 1985, Observation of shear waves and correletion with P-events. In Seismic Shear Waves, G. Dohr, (ed.), Handbook of Geophysical Exploration, **15b**, Geophysical Press.

Li, X. and Yuan, J., 2001, Converted-wave imaging in inhomogeneous, anisotropic media: EAGE, 63rd Conference and Technical Exhibition, Amsterdam, The Netherlands.

McCormark, M.D., Dunbar, J.A. and Sharp, W.W., 1984, A case study of stratigraphic interpretation using shear and compressional seismic data: Geophysics, **49**, 409-520.

Stewart, R.R. and Ferguson, R.J., 1996, Shear-wave interval velocity from P-S stacking velocities: Canadian Journal of Exploration Geophysics, **32**, 139-142.

Stewart, R.R., Gaiser, J.E., Brown, R.J. and Lawton, D.C., 2003, Converted-wave seismic exploration: Applications: Geophysics, **68**, 40-57.

Tanner, M.T. and Koehler, F., 1969, Velocity spectral-digital computer derivation and application of velocity functions: Geophysics, **34**, 859-881.

Tessmer, G. and Behle, A., 1988, Common reflection point data-stacking technique for converted waves: Geophysical Prospecting, **36**, 671-688.

Thomsen, L., 1999, Converted-wave reflection seismology over inhomogeneous, anisotropic media: Geophysics, **64**, 678-690.

Thickness = 5000 m

V_P = 3600 m/s

V_S = 1200 m/s

ρ = 2.2 g/cm^3

V_P = 12000 m/s

V_S = 6000 m/s
ρ = 2.6 g/cm^3

FIG. 1. A single layer geologic model used in testing Equation 3.

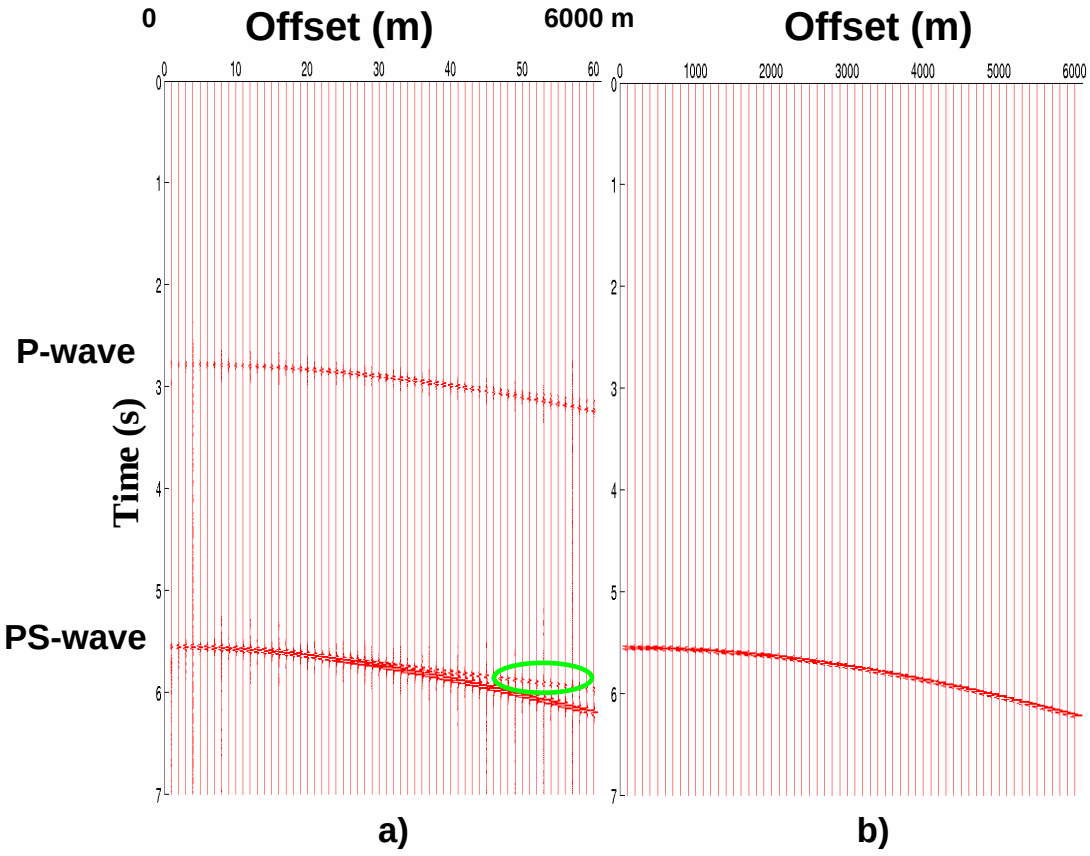

FIG. 2. (a) Synthetic shot record from ANIVEC. Circled in green is a P-wave refracted event from the layer boundary. (b) Synthetic seismograms from Equation 3.

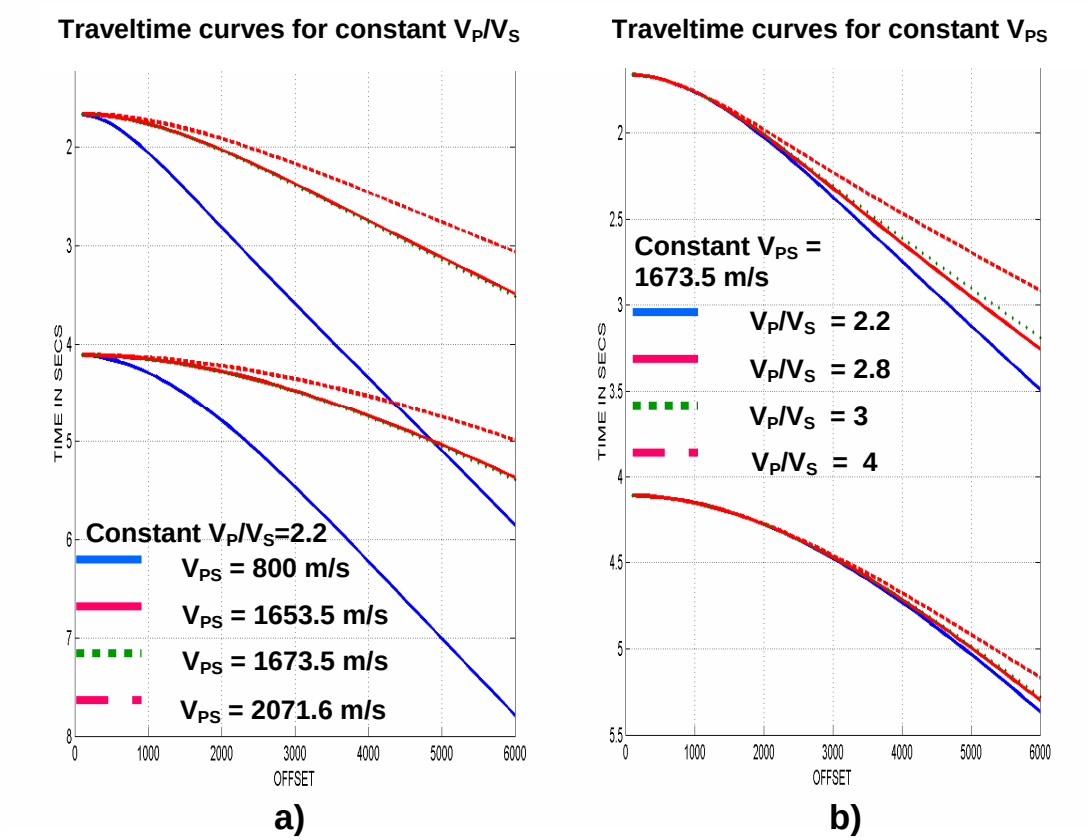

FIG. 3. Sensitivity test: (a) Traveltime curves for variable velocities with fixed γ_0; (b) Traveltime curves for variable γ_0 but fixed velocity.

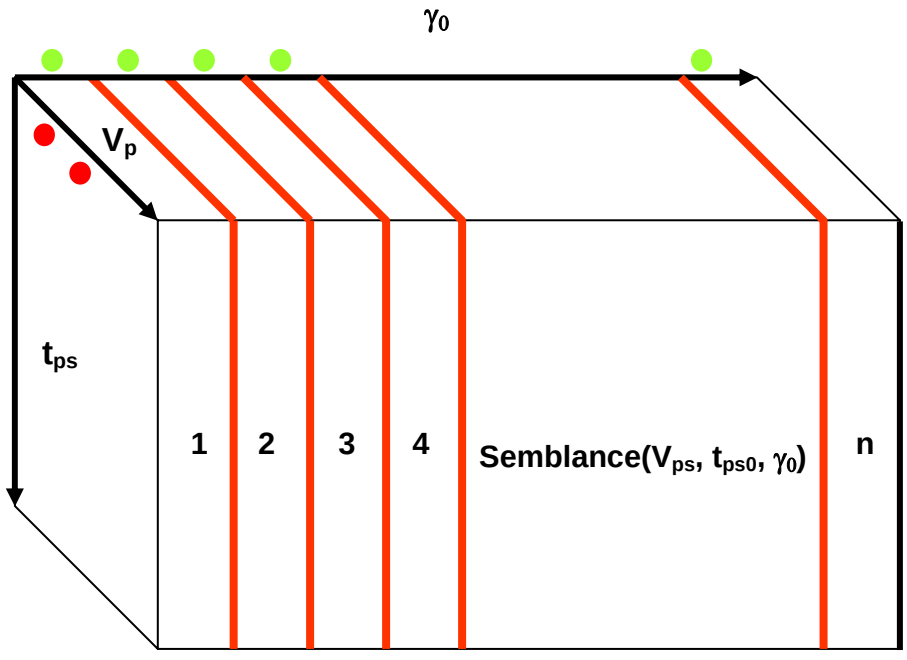

FIG. 4. Schematic demonstrating the scanning code concept. Red dots represent semblance values on the semblance plane; while the green dots represent average γ_0.

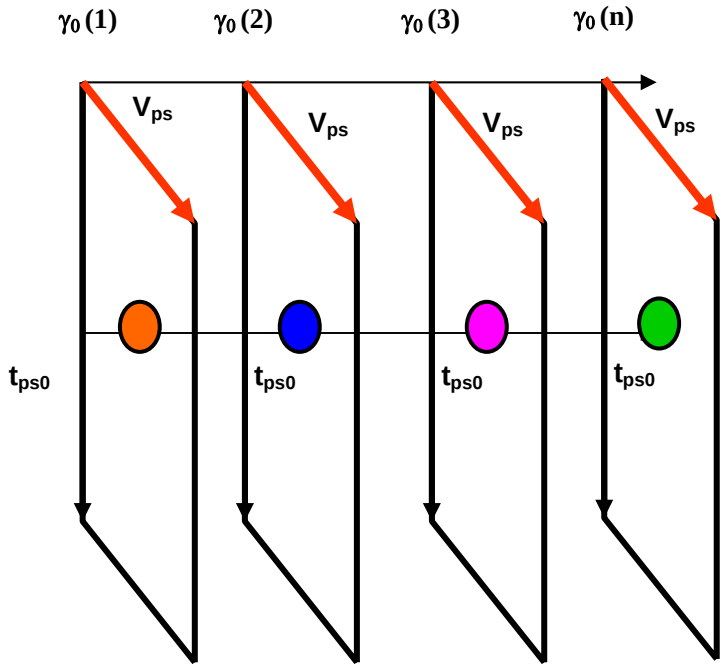

FIG. 5. Schematic illustrating the scanning algorithm; each panel represents a 2D semblance panel from each sub-volume; the colored dots red, blue, magenta and green represent different semblance values on the 2D panels from which maximum semblance value is selected at each zero-offset time and the corresponding V_{PS}. The selected value is output onto the final 2D semblance panel while the corresponding γ_0 value is output onto the γ_0 panel (see Figure 6).

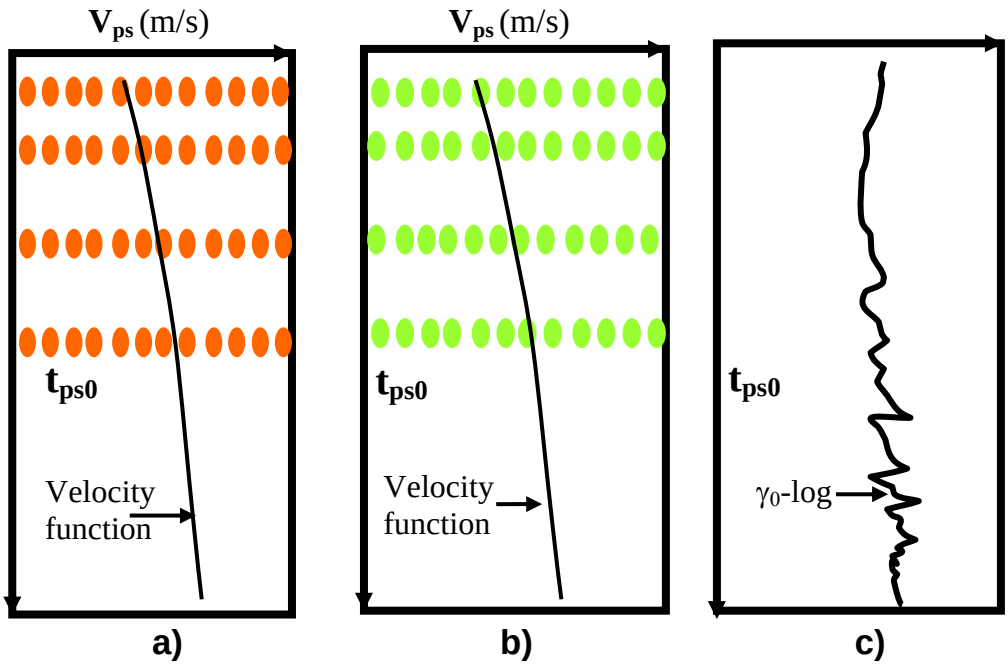

FIG. 6. Schematic illustrating the scanning algorithm; (a) Final 2D semblance panel with picked velocity function; (b) 2D γ_0 panel containing the scanned γ_0 values and the transferred velocity function; (c) plotted γ_0-log representing γ_0 values encountered by the velocity function.

Thickness = 1000 m **V_P = 3000 m/s**	**V_S = 1395 m/s** **ρ = 2.5 g/cm^3**
Thickness = 900 m **V_P = 3500 m/s**	**V_S = 1636 m/s** **ρ = 2.52 g/cm^3**
Thickness = 1700 m **V_P = 4000 m/s**	**V_S = 1878 m/s** **ρ = 2.54 g/cm^3**

FIG. 7. A geologic model used testing the V_P/V_S scanning algorithm. Model was generated in GX2 ray tracing package.

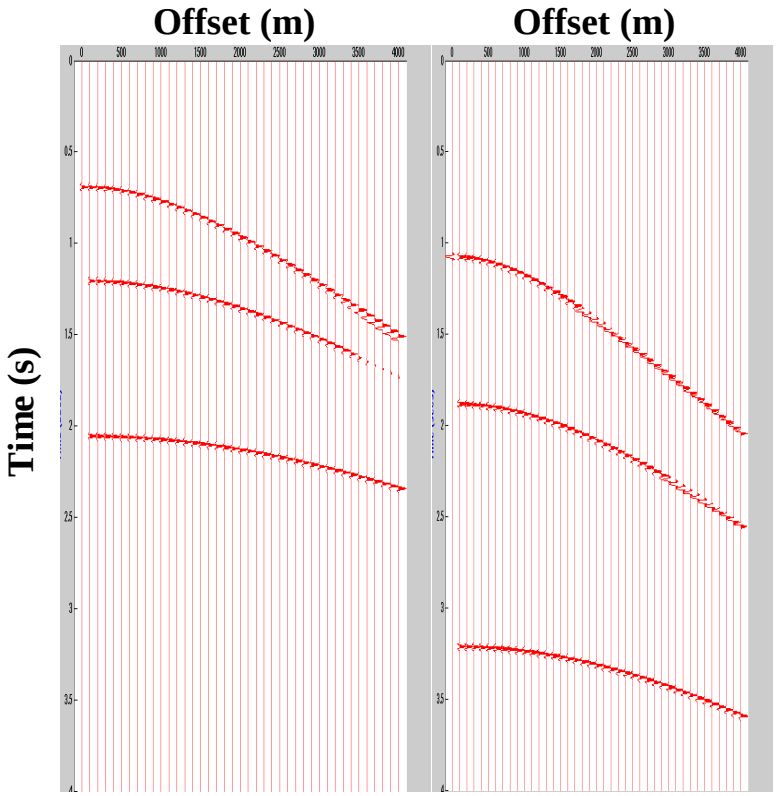

FIG. 8. Examples of shot records obtained from the model shown in Figure 7; (a) *P*-wave shot record, (b) *PS*-wave shot record.

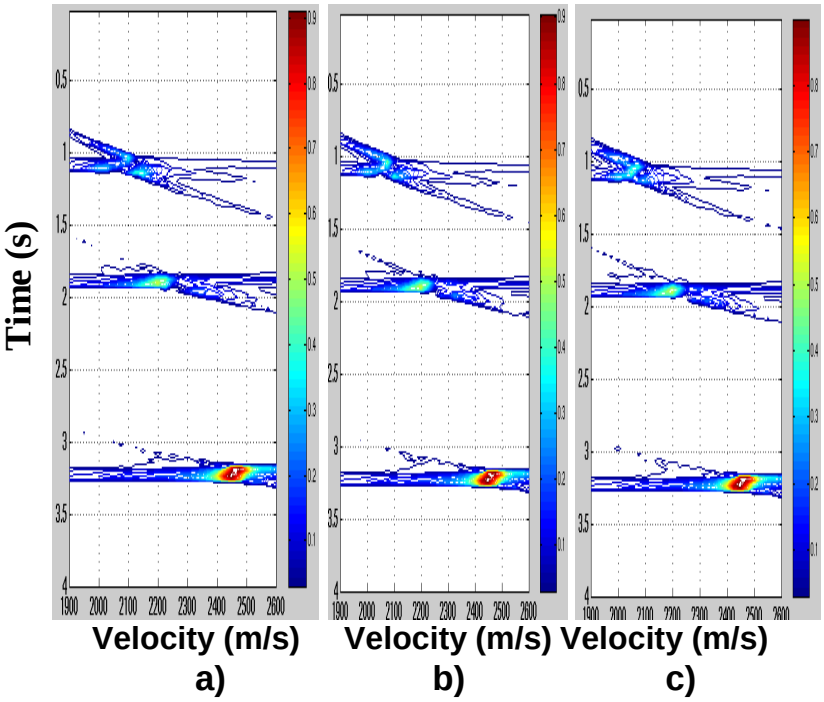

FIG. 9. 2D display of velocity semblance from 3 sub-volumes: (a) sub-volume 1, (b) sub-volume 4 and (c) sub-volume 6. From (a) to (c), there is a progressive increase in maximum semblance at the various levels. Moveout velocity variation is more pronounced at the shallowest level. At the three horizons, there is better focusing of maximum semblance in sub-volume 6 (c).

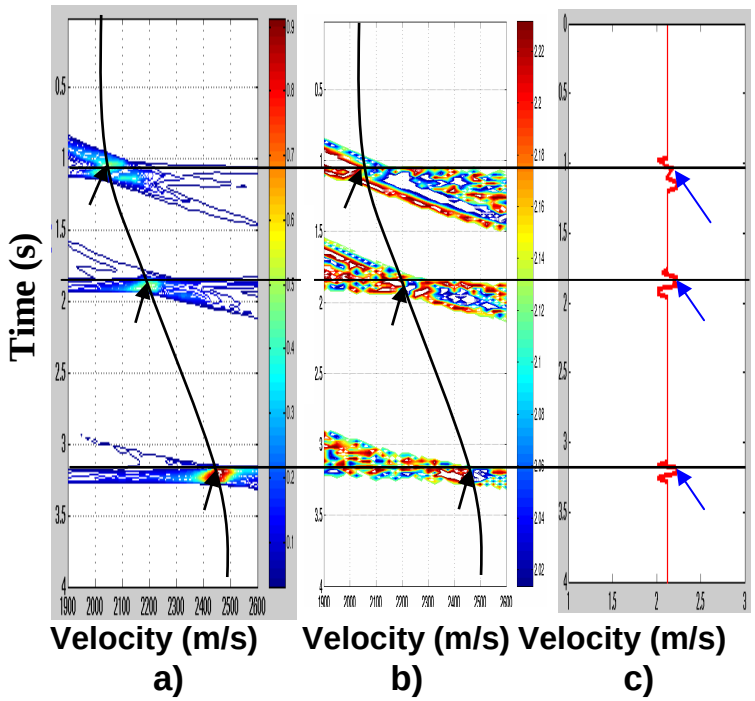

FIG. 10. (a) Final 2D velocity semblance display with picked velocity function (black curve); (b) Scanned velocity ratio (γ_0) panel with picked velocity function (black curve); (c) Plot of γ_0 versus time. In the semblance plot (a), the black arrows indicate locations of picked maximum semblance; while in (b), the arrows indicate the same coordinate locations where corresponding γ_0 values are picked. In (c), the blue arrows indicate the values of picked γ_0.

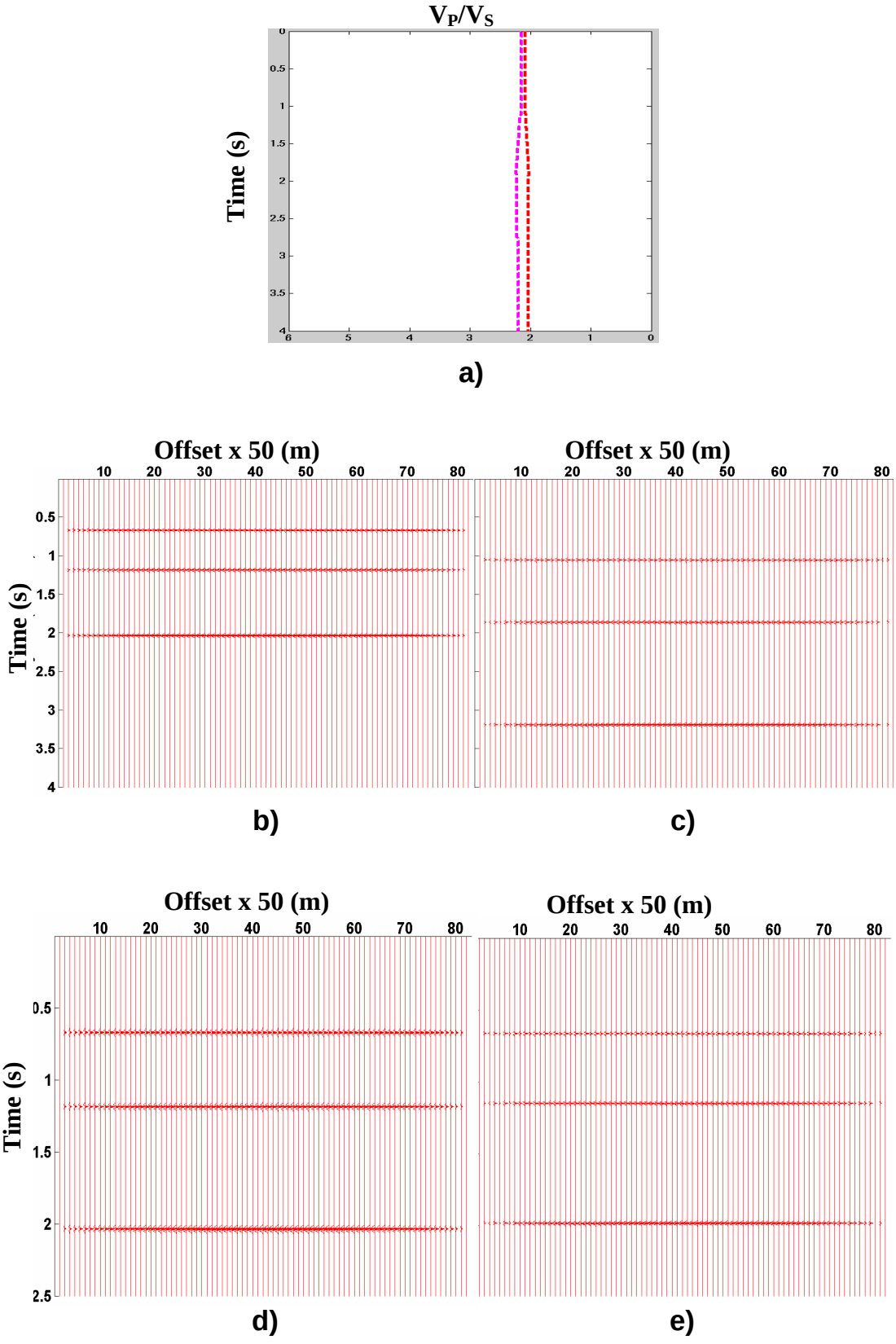

FIG. 11. (a) V_P/V_S versus time plot, (b) *PP* stacked section, (c) *PS* stacked section, (d) is a *PP* stacked section compared to the transformed *PS*-stacked section (e).

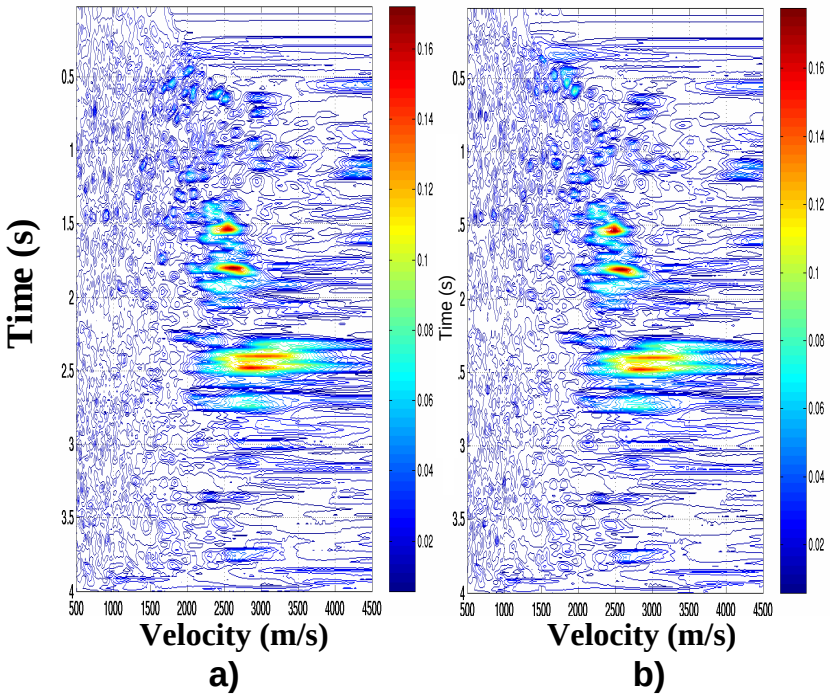

FIG. 12. (a) Velocity semblance from panel 1, (b) Velocity semblance from panel 11. The V_P/V_S values used in generating these panels are respectively 1.5 and 2.8.

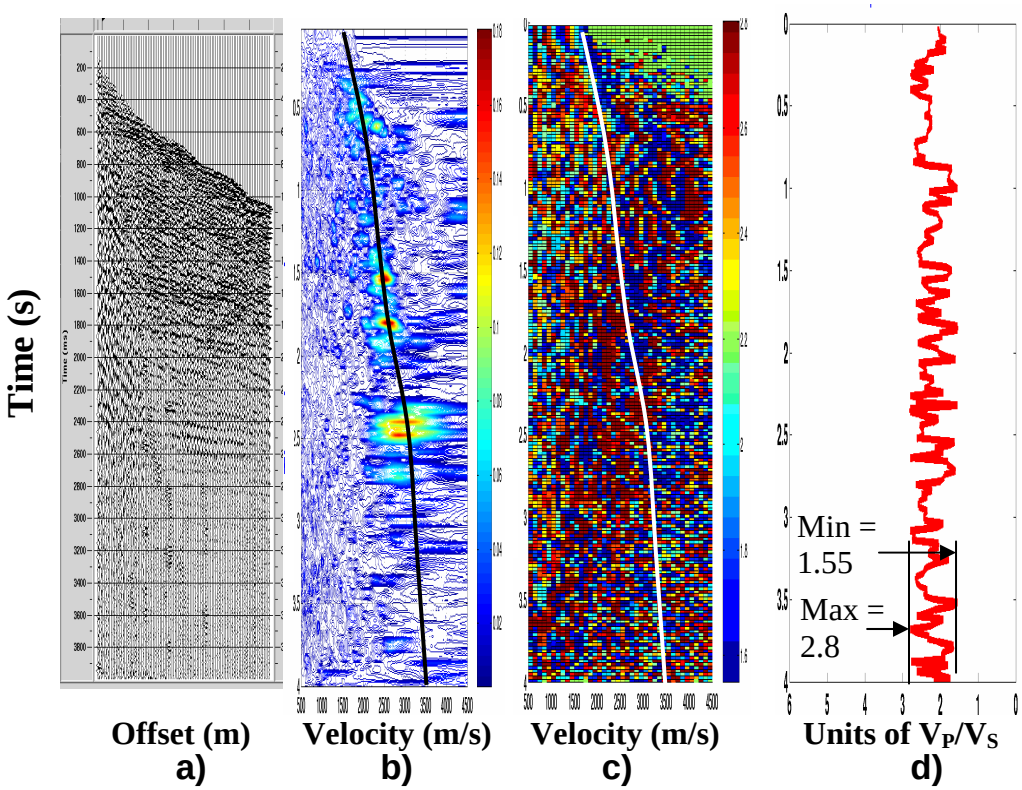

FIG. 13. (a) Asymptotic common point (ACP) 350 gather at Well 09-08 location, (b) Final 2D velocity semblance with picked velocity function (black curve); the scale of the colorbar varies from 0.0 to 0.18. (c) 2D velocity ratio panel with transferred velocity function (white curve); the scale of the colorbar range from 1.5 to 2.8. (d) Automatically plotted velocity ratio values versus corresponding time log (γ_0-log) from (c).

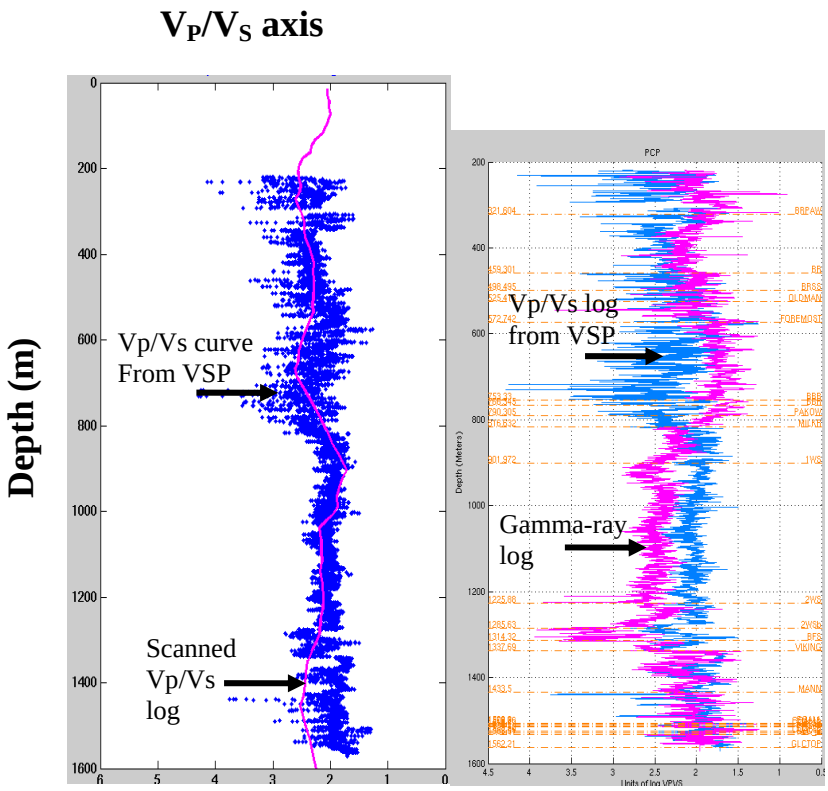

FIG. 14. Comparison of scanned V_P/V_S log with VSP V_P/V_S log from Well 09-08. (a) Scanned V_P/V_S log (purple curve) superimposed on V_P/V_S log from Well 09-08 (blue curve). (b) Well 09-08 gamma-ray log (pink curve) plotted with V_P/V_S log (blue curve). See text for details.

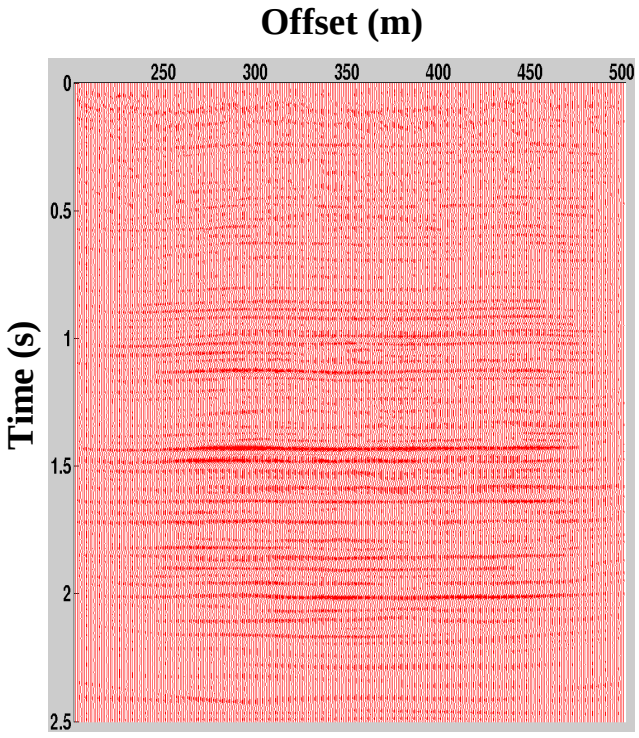

FIG. 15. P-wave stacked section from the Blackfoot oil field obtained from ProMAX.

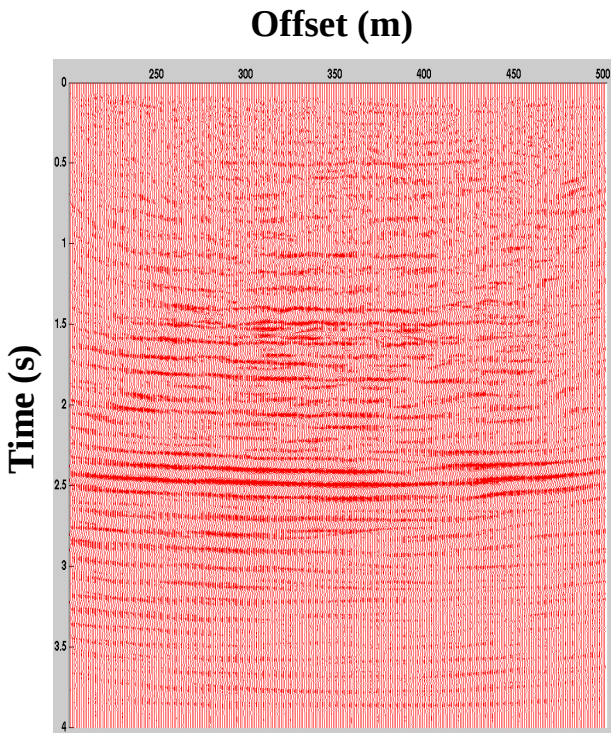

FIG. 16. *PS*-wave stacked section from the Blackfoot oil field obtained from ProMAX prior to transformation to *P*-wave times.

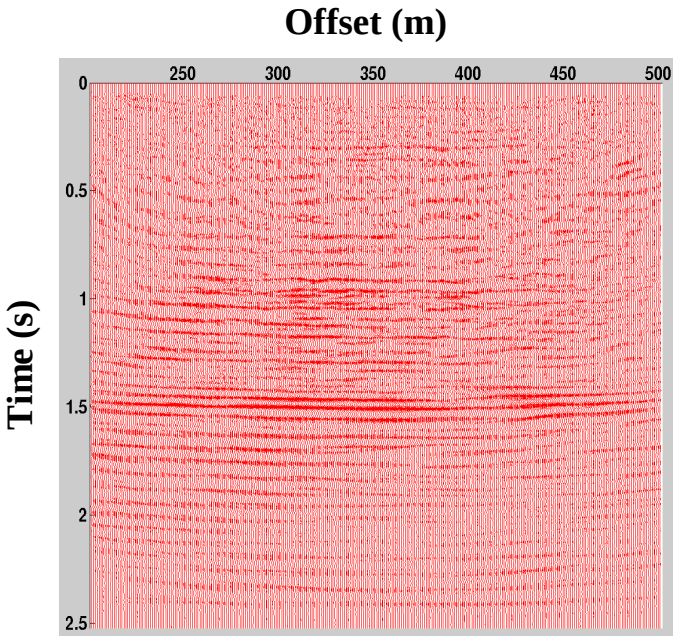

FIG. 17. *PS*-wave stacked section from the Blackfoot oil field obtained from ProMAX after transformation to *P*-wave times in Matlab.

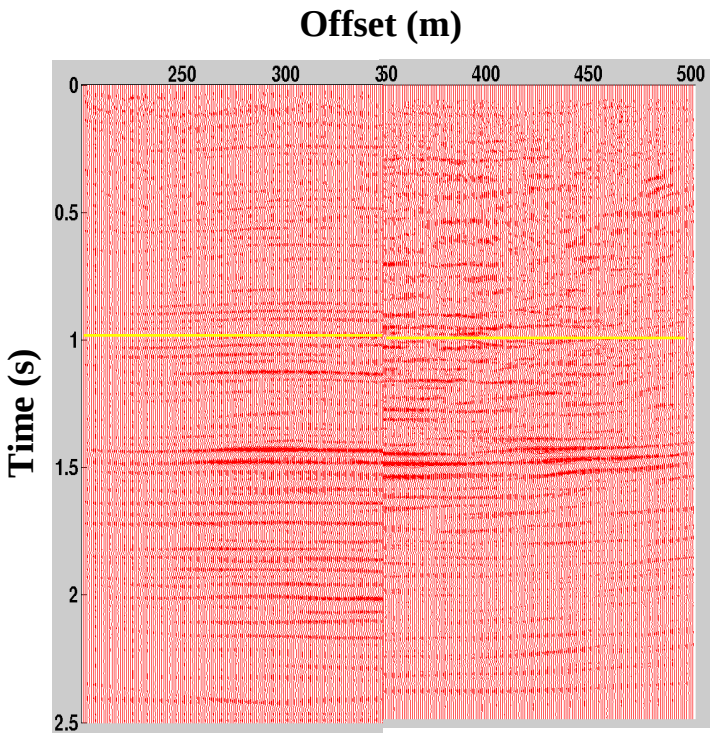

FIG. 18. Comparison of the transformed *PS* stacked section with the *P*-wave stacked section. (a) Part of the *PP* stacked section spliced onto a part (b) of the transformed *PS* stacked section at the Well 09-08 location (CDP 350).

Table 1. Comparison of traveltimes: from ANIVEC and Equation 3 for the first 10 offsets. Average error is -0.04%.

Offsets	**1**	**2**	**3**	**4**	**5**	**6**	**7**	**8**	**9**	**10**
Eqn. (3)	**5.5558**	**5.5564**	**5.5575**	**5.5589**	**5.5608**	**5.5631**	**5.5658**	**5.5689**	**5.5724**	**5.5764**
ANIVEC	**5.5720**	**5.5760**	**5.5760**	**5.5760**	**5.5800**	**5.5840**	**5.5880**	**5.5920**	**5.5960**	**5.6000**

Table 2. Comparison of traveltimes: from ANIVEC and Equation 3 for the last 10 offsets. Average error is -0.4%.

Offsets	**1**	**2**	**3**	**4**	**5**	**6**	**7**	**8**	**9**	**10**
Eqn. (3)	**6.0508**	**6.0687**	**6.0868**	**6.1052**	**6.1238**	**6.1426**	**6.1616**	**6.1809**	**6.2003**	**6.2199**
ANIVEC	**6.2520**	**6.2800**	**6.3040**	**6.3320**	**6.3600**	**6.3840**	**6.4120**	**6.4400**	**6.4680**	**6.4960**

Table 3. Computed traveltimes and velocity ratios. The t_{p0}, t_{s0}, and t_{ps0} are respectively the *P*-, *S*- and *PS*-wave two-way time within each layer.

Thickness (m)	**t_{po} (s)**	**t_{so} (s)**	**t_{pso} (s)**	**t_{so}/ t_{po} (s)**
1000	**0.6666**	**1.4334**	**1.0500**	**2.15**
900	**1.1808**	**2.5340**	**1.8574**	**2.15**
1700	**2.0308**	**4.3446**	**3.1877**	**2.14**

Table 4. Computed velocities: V_{Pint} and V_{Sint} are respectively the *P*- and *S*-wave interval velocities while the others are as defined earlier on.

Thickness (m)	V_{po} (m/s)	V_{so} (m/s)	V_{prms} (m/s)	V_{srms} (m/s)	V_{psrms} (m/s)
1000	3000	1395	3000	1395	2046
900	3500	1636	3227	1504	2203
1700	4000	1878	3571	1670	2442

Table 5. Scanned velocity ratios and *PS* velocities (V_{PS}).

Horizon	t_{ps} (s)	V_{ps} (m/s)	Scanned γ_0
1	1.0500	2040	2.16
2	1.8574	2200	2.23
3	3.1877	2450	2.21

Table 6. Differences between the input and scanned γ_0

Horizon	scanned γ_0	Input γ_0	Difference
1	2.16	2.15	0.01
2	2.23	2.15	0.08
3	2.21	2.14	0.07

Table 7. Differences between the input and scanned velocities (V_{PS}).

Horizon	scanned V_{ps} (m/s)	Input V_{ps} (m/s) γ_0	Difference	% Difference
1	**2040**	**2046**	**+ 4**	**- 0.3**
2	**2200**	**2203**	**- 3**	**- 0.1**
3	**2450**	**2450**	**0**	**0.0**

Table 8. Differences between actual and derived *P*-wave times

Horizon	Derived t_{p0} (s)	Actual t_{p0} (s)	Difference	% Difference
1	**0.6650**	**0.6666**	**- 0.0016**	**- 0.2**
2	**1.1500**	**1.1808**	**- 0.0308**	**- 3.0**
3	**1.9861**	**2.0308**	**- 0.0447**	**-2.0**